PNAS RESEARCH ARTICLE | NEUROSCIENCE

Saccade-related LFP power transients in the primate amygdala and hippocampus linked to the perception of social status

SeungHyun Lee[a], Hanga Dormán[b], Zoltan Nádasdy[c,d,e], and Katalin M. Gothard[b,1]

Affiliations are included on p. 10.

Edited by Elizabeth Buffalo, University of Washington School of Medicine, Seattle, WA; received June 21, 2025; accepted December 4, 2025

A key aspect of healthy social functioning in both humans and nonhuman primates is the ability to extract status-related information from observing the social signals exchanged between individuals. Knowing the social status of others determines how long we look at them and how we engage with them in social interactions. While looking at faces and eyes requires a functionally intact amygdala, hippocampal memories guide the eyes toward socially relevant areas of a visual scene. We examined the local field potentials associated with socially meaningful eye movements in the amygdala and hippocampus of macaques as they watched videos of dominant–subordinate interactions among unfamiliar conspecifics. In both structures, the saccade-related potentials showed status-dependent amplitude modulation in specific frequency bands. In the amygdala, shifting gaze from lower- to higher-status individuals was associated with anticipatory power transients in the 20 to 25 Hz frequency band, whereas gaze shifts from higher- to lower-status individuals were marked by predominantly postsaccadic power transients. Following the gaze of the aggressive, dominant individual induced increased postsaccadic power in the gamma band in both the amygdala and hippocampus, with some variation in frequency depending on whether the saccade landed on the social partner or elsewhere. The timing, frequency, and status-specificity of these power transients reveal the contribution of the amygdala and hippocampus to the visual exploration of social scenes.

macaques | scanpath | gaze following | gamma band | beta band

Significance

During natural vision, the spontaneous sequence of saccades reveals the viewer's priorities for allocating visual attention to meaningful details. We recorded perisaccadic neural activity in the amygdala and hippocampus of macaques while they viewed videos of simulated social interactions between dominant–subordinate pairs of individuals. Social status predicted the presence, timing, and frequency components of transient changes in the local field potentials in both regions. Presaccadic power transients predicted the status of the individual targeted by upcoming saccades, suggesting that the amygdala is tuned to features of the social scene that are preselected for future fixations. These findings confirm the presence of a status-related variable in the primate amygdala that may orchestrate the visual exploration of social scenes.

Visual and cognitive mechanisms mediated by the primate amygdala and hippocampus support social learning, particularly the processes involved in discerning the social status of individuals within hierarchical societies (1–3). Under natural conditions, when direct interactions with all group members are not possible, status learning occurs through observation (4–6). Converging evidence suggests that the sequence of fixations and saccades made by observers convey information both about their prior social knowledge and about the predictions acquired through learning (3, 7–10). Observers of social interactions often fixate on dominance cues such as gaze direction, posture, gestures, and facial expressions (11–13). The amygdala decodes many of these social signals (14, 15), and its damage or removal consistently disrupts the natural tendency to look at the eyes of others (16, 17). Visual attention to the eyes not only provides the richest facial information but also enables gaze-mediated social behaviors such as gaze following and joint attention (18, 19). These eye movements reveal a basic mechanism of understanding the mental states of others (20). Although the amygdala is not part of the core oculomotor network, it is functionally embedded in a broader eye-movement circuit (21). It influences when and where primates look, especially in social or emotionally salient contexts, through projections to the basal ganglia–superior colliculus loop and interactions with cortical oculomotor areas (22).

During natural vision, when the viewer's gaze is fixated on a detail such as the right eye of a face, a covert shift of attention toward the next saccade target enhances processing of that location. This phenomenon, known as predictive remapping, is an anticipatory signal that tunes visual processing to the features of the upcoming target even before the saccade occurs (23–25). This remapping of receptive fields is evident in early visual cortex V1 and V2 (26), in V4 (27) and frontal eye field (28). The frontoparietal oculomotor pathways responsible for predictive remapping typically omit the amygdala and medial temporal lobe (29). However, based on its role in processing social status and the face-viewing deficits induced by amygdala lesions, we hypothesized that the dynamic interplay between feedforward (unpredicted, currently processed) and feedback (predicted, anticipatory) signals has a neurophysiological signature in the local field potentials (LFPs) therein. Accordingly, we examined perisaccadic neural activity in the amygdala while macaques observed dyadic social interactions between dominant and subordinate individuals and generated gaze-following (GF) and joint-attention (JA) saccades. Given the established

Author contributions: S.L. and K.M.G. designed research; S.L., H.D., Z.N., and K.M.G. analyzed data; and S.L., H.D., Z.N., and K.M.G. wrote the paper.

The authors declare no competing interest.

This article is a PNAS Direct Submission.

[1]To whom correspondence may be addressed. Email: kgothard@arizona.edu.

This article contains supporting information online at https://www.pnas.org/lookup/suppl/doi:10.1073/pnas.2516365123/-/DCSupplemental.

Published January 2, 2026.

link between the primate hippocampus and gaze behavior (30–32) we also examined saccade-related transients in the LFPs recorded from the anterior hippocampus.

Results

The subject monkeys watched 15-s videos of simulated pairwise interactions between members of a simulated linear hierarchy and learned the status of the protagonists (Fig. 1*A*). Juxtaposed videos, one showing a threatening monkey and the other an appeasing monkey, positioned to appear within each other's line of sight simulated social interactions. Facial expressions were timed to create a dynamic exchange of dominant–subordinate signals. From the observers' scanpaths, we extracted classes of saccades that shifted the viewers' attention from one monkey to the other (Fig. 1*B*). We distinguished between gaze-following (GF) and joint-attention (JA) saccades (Fig. 1*C*; see *Methods* for saccade classification criteria and *SI Appendix*, Fig. S1 for saccade and fixation duration statistics). Saccade dynamics were similar across subjects, showing the expected main-sequence relationship with comparable velocity–amplitude scaling. Intersaccade interval distributions for dominant and subordinate targets were largely similar, with only minor differences (*SI Appendix*, Fig. S2).

The viewers learned the status of the protagonists, as they looked longer and more frequently at the dominant monkey (Fig. 1*D*). Fixations preceding saccades within the face or body of the same monkey were longer than fixations preceding gaze shifts to the partner (Fig. 1*E*). Fig. 1*F* shows that while fixation durations before JA saccades did not differ significantly by the target's social status, JA saccades initiated from the subordinate were more frequent than those initiated from the dominant, as previously reported (9). This finding suggests that the viewers engaged in mentalizing with the protagonists, with elevated attention on the subordinate's appeasing displays toward the dominant partner. On the other hand, although fixation durations were slightly longer before GF saccades initiated from the dominant, they were initiated from the subordinate with equal probability, which is expected as these saccades do not land on the partner and therefore carry less social relevance. Next, we examined the neurophysiological underpinnings of these socially driven saccades.

Event-Related Potentials Reflect the Social Content of Videos. We analyzed the LFPs from two monkeys, M_A and M_D, recorded using 32-channel linear arrays lowered into the amygdala and the anterior hippocampus (Fig. 2*A*). The contacts were distributed along a 6.5 mm length of the shaft, allowing us to collect signals from multiple nuclei of the amygdala and regions of the anterior hippocampus immediately posterior to the amygdala that span 2 to 7 mm along the longitudinal axis of the hippocampus (see *SI Appendix*, Table S1 for recording sites in the amygdala and hippocampus and the topographic reconstruction of the electrode placement). We separately analyzed signals recorded from the centromedial (CMA) and basolateral (BLA) group of amygdala nuclei and various subregions of the anterior hippocampus (HIPP) (see *Methods* and *SI Appendix*, Table S2 for the details). To eliminate potential contamination from the ocular dipole and electromyographic activity of the contracting ocular muscles, we applied common average referencing (CAR) (33) (Fig. 2*B*), so that the resulting signal represents the neural activity of a local, mesoscale network of neurons (34, 35).

We compared the event-related potentials (ERPs) elicited by saccades and the subsequent fixations made by the viewers while: 1) watching videos of interacting monkeys, 2) watching videos of moving objects, and 3) looking at a blank screen between trial blocks. We contrasted ERPs during: 1) eye movements targeting dominant vs. subordinate individuals in the monkey videos (Fig. 2*C*), 2) monkey videos vs. object videos (Fig. 2*D*), and 3) any videos vs. the blank screen (Fig. 2*E*). We found that ERPs differentiated between stimuli across all three comparison types. In both nuclear groups of the amygdala—the CMA and BLA—ERPs triggered by saccades targeting dominant vs. subordinate monkeys showed amplitude differences in the 200 to 300 ms period after saccade onset. In the hippocampus, status-related differences emerged earlier, around 50 ms after saccade onset (Fig. 2*C*). When contrasting ERPs associated with social vs. object stimuli, we found less prominent but consistent differences approximately 200 ms postsaccade across all regions, along with additional transient differences in the CMA (Fig. 2*D*).

Across all three anatomical regions, the largest ERP difference was marked when contrasting videos with blank screen saccades, highlighting both visual and nonvisual components of the perisaccadic ERP modulation. The postsaccadic deflections of the ERPs in the amygdala and the hippocampus corresponded to a short theta burst lasting approximately one cycle (200 to 250 ms, 4 to 5 Hz). This replicates previous findings in the hippocampus, where saccades are followed by a theta burst that is independent of the saccade target and present even in the dark (31, 32, 35).

Social Status Determines the Spectral Signature of Gaze Shifts in the Amygdala. To explore the relationship between social status and saccade-related modulations of oscillatory power, we compared the time–frequency spectra of LFPs centered around the onset of saccades targeting the dominant or subordinate animals (Fig. 3*A*). Although the LFPs contained multiple frequency bands with excess power relative to the 1/f curve fitted to the power spectrum (*SI Appendix*, Fig. S3), social gaze-related changes were confined to the 20 to 40 Hz range. As shown in Fig. 2*B*, LFPs were grouped based on their anatomical provenance in two main nuclear groups of the amygdala, CMA and BLA, and the hippocampus. Time–frequency heatmaps (TFHs) were aligned to eight different types of saccades based on their origin and target. In addition, we separately analyzed saccades associated with GF with the dominant (GFD) or subordinate (GFS), and JA with the dominant (JAD) or subordinate (JAS).

To isolate the influence of social hierarchy, we subtracted the mean TFH of saccades that stayed within the same target monkey from the mean TFH of saccades made to a different target monkey because the latter represented an attentional shift to a monkey with a different social status. The subtraction unmasked the net effect of gaze switching on the spectral dynamics by removing the saccade effect unrelated to social status. We refer to the TFHs obtained by subtraction as TFH differences or TFHDs for short. This generated two contrasts for social hierarchy: DS–DD and SD–SS. Likewise, two contrasts, GFD–GFS, and JAD–JAS, were computed to assess social hierarchy effects in GF and JA conditions, respectively (*SI Appendix*, Fig. S4). These contrasts revealed multiple hierarchy-dependent effects on saccade-related LFPs. For example, the TFHD resulting from the DS-DD subtraction contains features unique to saccades directed toward the subordinate relative to saccades to the dominant, while removing the features common to all other saccades that stayed within the dominant target. Conversely, SD–SS contrast represents unique changes in the power spectrum caused by switching gaze from the subordinate to the dominant, while removing features associated with all saccades originating and targeting the subordinate. In the case of GF and JA saccades, the subtractions unmask the effect of the social status of the monkey driving the subject's gaze on the power spectrum.

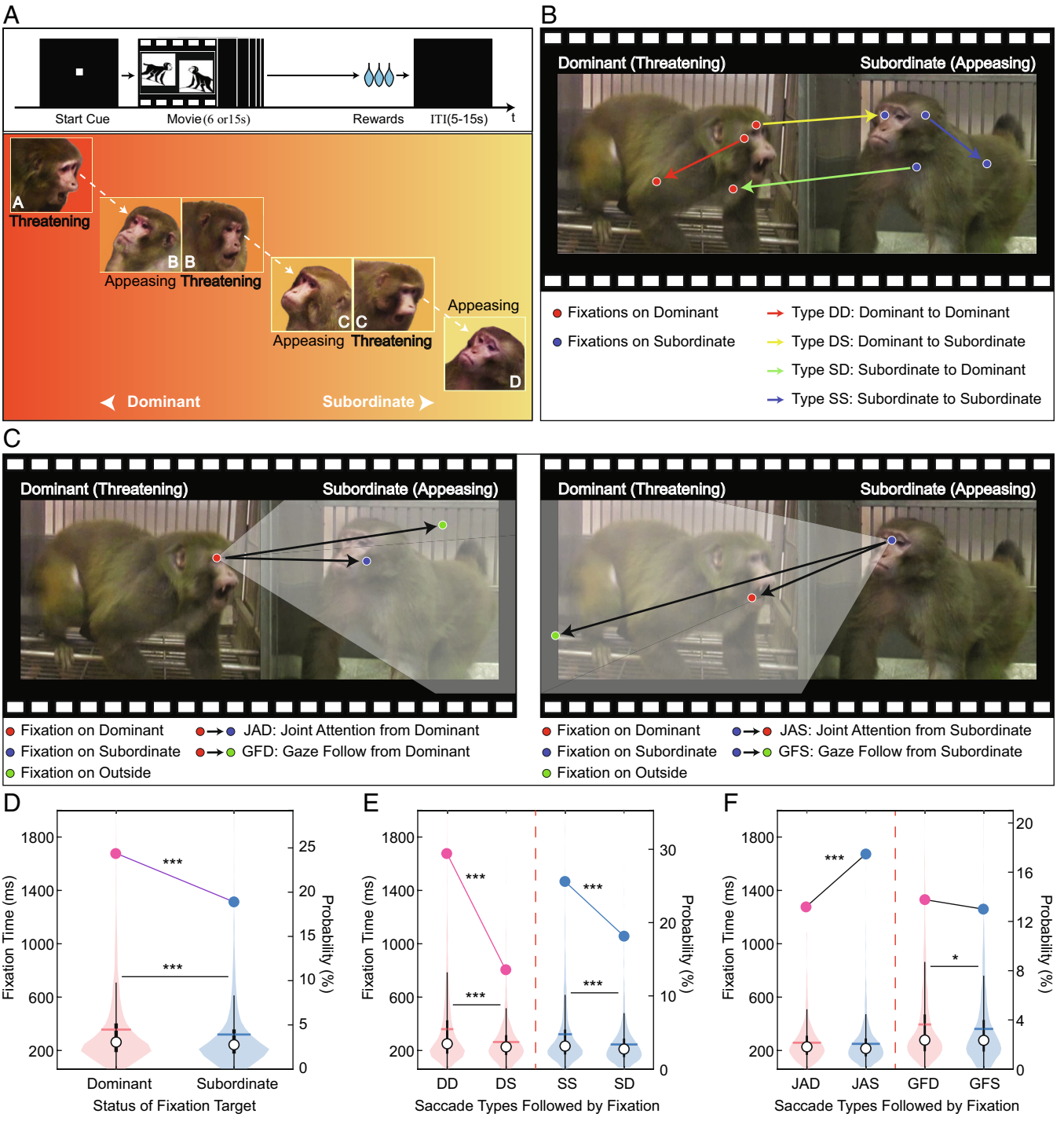

Fig. 1. Subjects decode social status from videos of simulated hierarchical interactions and exhibit socially driven eye movements. (*A*) Trial flow and hierarchy group composition. Each trial began with a 250-ms fixation on a start cue. The viewers were free to scan the video or look away during playback. After each video, the viewer received the same amount of reward regardless of video type. An example linear hierarchy of four male monkeys (A, B, C, and D) is shown, where the top-ranking monkey A consistently appears threatening and the bottom-ranking monkey D appears consistently appeasing. Mid-ranking monkeys B and C appear either threatening or appeasing depending on the status of their social partner. (*B*) Classification rule and examples for four different types of saccades, depending on the social status of the saccade origin and the fixation target: DD = from dominant to dominant; DS = from dominant to subordinate; SS = from subordinate to subordinate; SD = from subordinate to dominant. (*C*) Classification rules and examples for JA and GF saccades: JAD = JA saccades from the face area of dominant; JAS = JA saccades from the face area of subordinate; GFD = GF saccades from the face area of dominant; GFS = GF saccades from the face area of subordinate. (*D–F*) Distribution of fixation times (violin plots, left y-axis) and relative frequency of different saccade types (solid dots, right y-axis). *** and * indicate significant differences at $P < 0.001$ and $P < 0.05$, respectively. (*D*) Grouping by the social status of the fixation target (dominant vs. subordinate): t(16652) = 8.11, SD = 290.69, $P = 5.4e\text{-}16$; $\chi^2(1) = 530.61$, $P = 2.1e\text{-}117$. (*E*) Grouping by both the origin and target of saccades: DD vs. DS, t(4031) = 10.26, SD = 277.93, $P = 2.2e\text{-}24$; $\chi^2(1) = 698.45$, $P = 6.5e\text{-}154$. SS vs. SD, t(3183) = 9.01, SD = 236.18, $P = 3.5e\text{-}19$; $\chi^2(1) = 118.51$, $P = 1.3e\text{-}27$. (*F*) Grouping by JA and GF saccades: JAD vs. JAS, t(1691) = 1.45, SD = 148.30, $P = 0.15$; $\chi^2(1) = 39.70$, $P = 3.0e\text{-}10$. GFD vs. GFS, t(1507) = 2.04, SD = 315.35, $P = 0.042$; $\chi^2(1) = 1.41$, $P = 0.24$.

The TFHDs in Fig. 3 illustrate the distribution of power during saccades that shift the viewer's gaze from the dominant to the subordinate (left columns) and from the subordinate to the dominant (right columns). In the CMA, the DS–DD and SD–SS contrasts revealed increased power in the 20 to 30 Hz frequency band (DS–DD, $P = 2.01e\text{-}35$, and SD–SS, $P = 5.13e\text{-}78$, Wilcoxon test). This

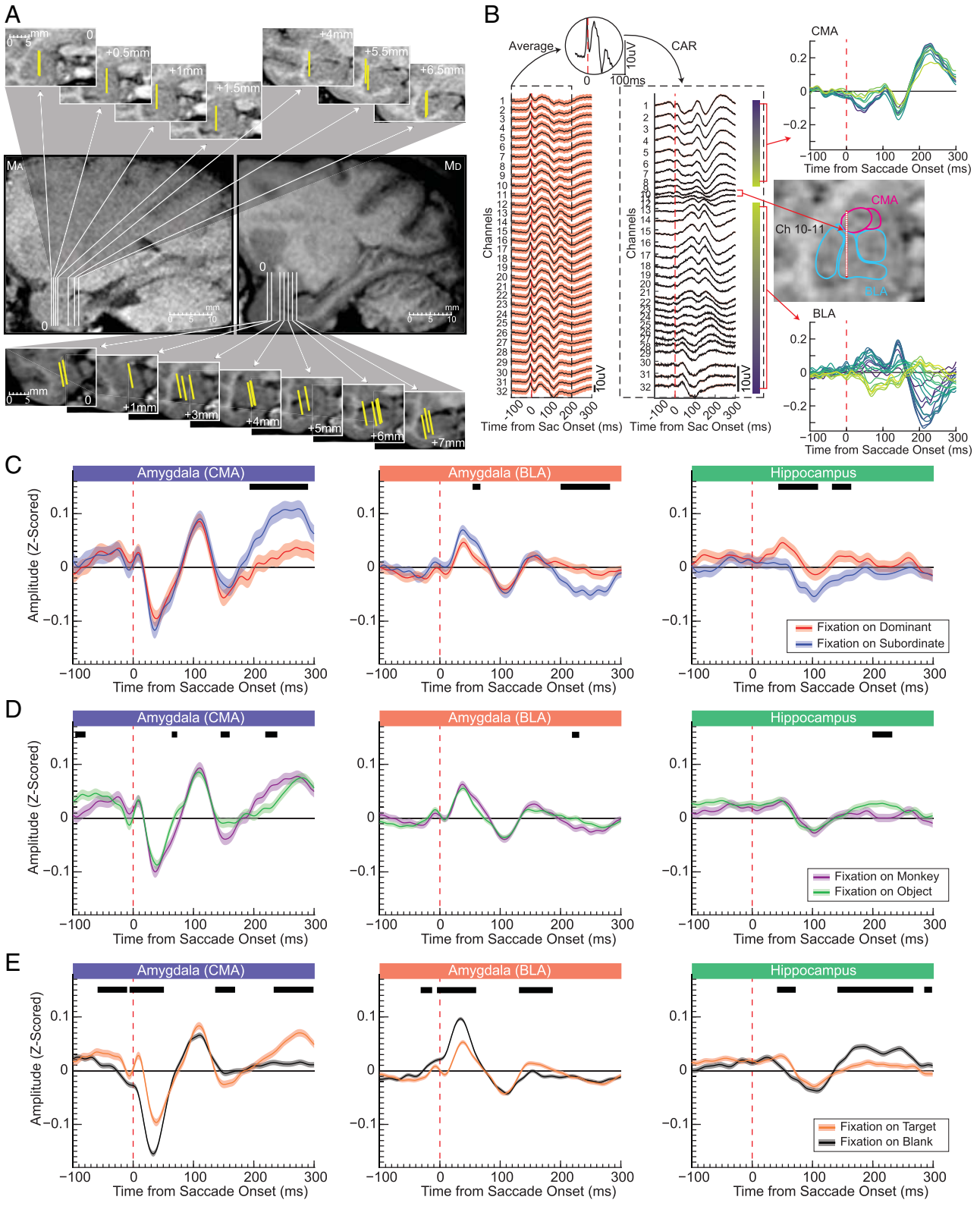

Fig. 2. Event-related potentials in the amygdala and hippocampus differentiate between stimulus types. (*A*) Recording locations in M_A (*Left* and *Top*) and M_D (*Right* and *Bottom*), showing the positions of the linear electrode arrays (yellow bars) across all 23 recorded sites over 20 recording days. (*B*) Example LFP data and preprocessing steps. Signals were aligned by saccade onset. Large deflections caused by the ocular dipole and the electrical activity of the ocular muscles were removed by subtracting a CAR signal, computed by averaging all 32 channels in the same electrode. The resulting traces represent LFPs, which varied across channels located in different nuclei of the amygdala. The *Inset* on the right shows the placement of the linear probe in the amygdala, with individual traces recorded from 8 channels in the CMA (above MRI reconstruction) and 16 channels located in different subdivisions of the BLA (below MRI reconstruction). (*C–E*) Saccade-aligned ERPs reflect the social relevance of the fixated visual stimuli. Broadband-filtered (0.1 to 50 Hz) LFPs were aligned to saccade onset and averaged across electrodes within regions (*Left*: CMA, *Middle*: BLA, *Right*: HIPP), as well as across subjects, trials, and saccades of the same type. Shaded areas represent SEM. Horizontal black line segments above waveforms indicate statistically significant differences between the respective saccade categories (two-sample Welch's *t* test, $\alpha = 0.05$); only differences continuously significant for at least 10 ms are shown. (*C*) ERPs from saccades targeting the dominant (red) vs. subordinate (blue). (*D*) ERPs from saccades driven by social (monkey videos, purple) vs. nonsocial (object videos, green) stimuli. (*E*) ERPs from stimulus-driven (orange) vs. blank screen (black) saccades.

power transient of 300 ms straddled the saccades, but the duration of pre- and postsaccadic portion depended on the social status of the target. Indeed, when the target was the subordinate, the power transient was predominantly postsaccadic. In contrast, a saccade to the dominant target was preceded by a predominantly presaccadic power transient at a lower frequency (Fig. 3*B*) as evident from the reversal of differences between the presaccadic and postsaccadic TFHDs (DS–DD, P = 5.65e-11, Wilcoxon test, P = 4.89e-20, Kruskal–Wallis test, Cohen's d = −0.64 and SD–SS P = 1.35e-22, Wilcoxon test P = 2.09e-21 Kruskal–Wallis test, Cohen's d = 0.98). Hence, the anticipated fixation on the dominant monkey elicited increased beta-gamma band activity before the onset of an upcoming saccade to the dominant monkey relative to a saccade within the subordinate monkey, on which the subject was originally fixated. This effect in the CMA was reproduced by the BLA (DS–DD P = 2.30e-05, Wilcoxon test, P = 1.45e-10 Kruskal–Wallis test, Cohen's d = −0.44 and SD–SS P = 1.07e-10, Wilcoxon test, P = 2.28e-06 Kruskal–Wallis test, Cohen's d = 0.48), along with the main beta-gamma increase ($P_{DS–DD}$ = 1.64e-40, $P_{SD–SS}$ = 4.51e-79, Wilcoxon tests) (Fig. 3*C*). Note that the TFHDs in the hippocampus (Fig. 3*D*) showed diffuse power differences extending from approximately 250 ms before to 100 ms after the saccade in both saccade types (DS–DD and SD–SS), which were markedly attenuated compared to the amygdala. Although the difference between the pre- and postsaccadic period was statistically significant, because the increase in power in the 20 to 25 Hz range begins around 250 ms prior to saccade onset, we cannot exclude the possibility that this activity reflects carry-over from the preceding fixation. The same analyses were performed separately for two viewer monkeys, and the reproducible patterns across subjects are illustrated in *SI Appendix*, Figs. S5 and S6. These results demonstrate that the individual patterns of perisaccadic LFP oscillations were consistent between the two monkeys, as summarized in *SI Appendix*, Table S3.

The Spectral Signatures of Gaze-Following and Joint-Attention Saccades in the Amygdala and the Hippocampus. Given the importance of gaze following and joint attention in natural social interactions, and how little is known about their neural

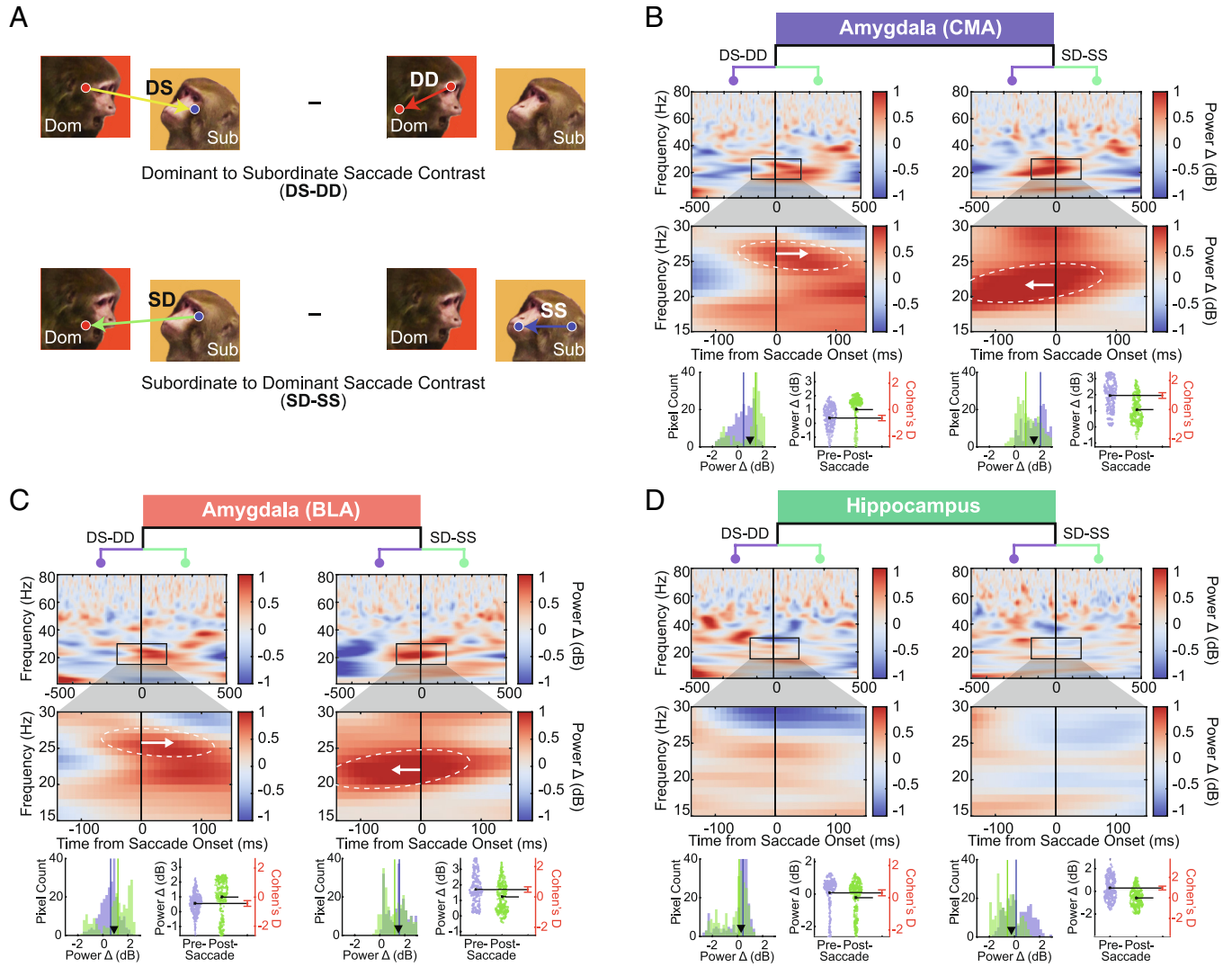

Fig. 3. The spectral signature of different saccade types. (*A*) Schematic of the dominant-to-subordinate (DS–DD, *Top*) and subordinate-to-dominant (SD–SS, *Bottom*) saccade contrasts used to compute the saccade-aligned TFHDs shown in panels *B*–*D*. (*B*) Saccade-related power transients in the TFHDs computed from the LFPs in the CMA. The magnitude of the difference (in dB) is mapped to the color scale shown on the right. To capture the most prominent effects, TFHDs in each panel are zoomed into a smaller time window (−150 ms to 150 ms centered on saccade onset) and frequency range (15 to 30 Hz). *Inset* plots below each TFHD show the distributions of pixel values in the presaccadic (purple) and postsaccadic (green) periods from two perspectives (*Left*), and the overall distribution across both (*Right*). Left columns: Difference between average TFHs of DS and DD saccades, i.e., the effect of switching gaze to the subordinate. Right columns: Difference between average TFHs of SD and SS saccades, i.e., the effect of switching gaze to the dominant. Under the distributions are Gardner-Altman plots of the data distributions and corresponding Cohen's D effect size estimates. (*C* and *D*) The same as in *B* for the BLA and the hippocampus, respectively.

substrate, we applied the same TFH contrasts to the subset of saccades that met the criteria for GF and JA saccades (*Methods*). As the targets of GF and JA saccades are different (both follow the gaze of the attended monkeys, but only JA saccades land on the face or body of the social partner), we separately compared the average TFHDs aligned to GFs of dominant vs. subordinate monkeys and carried out the same subtraction for the JAs. The observed status-related differences in timing, frequency band, and power represent the neurophysiological signature of these socially coordinated saccade types (Fig. 4). Specifically, these saccades were associated with increased postsaccadic LFP power in the gamma band (30 to 45 Hz) when the saccade targeted the dominant, clearly separated from the beta band when the saccade targeted the subordinate. In both nuclear groups of the amygdala (CMA and BLA) and in the hippocampus, positive postsaccadic power transients following GF and JA saccades directed at the dominant (GFD and JAD) occurred approximately 50 ms earlier than the equivalent positive transients for those saccades directed at the subordinate (Fig. 4 *B–D*). The same analyses were performed separately for two viewer monkeys, and the reproducible patterns across subjects are illustrated in *SI Appendix*, Figs. S7 and S8. These results demonstrate that the individual patterns of perisaccadic LFP oscillations were consistent between the two monkeys, as summarized in *SI Appendix*, Table S4.

These two effects—a presaccadic decrease and a postsaccadic increase in power—resulted in significant differences between the pre- and postsaccadic distributions of gamma and beta power for both GF and JA saccades in each region. In the CMA, significant differences were found for both GFD–GFS (P = 1.7e-4, Wilcoxon test, P = 7.46e-05, Kruskal–Wallis test, Cohen's d = −0.48) and JAD–JAS (P = 5.46e-25, Wilcoxon test, P = 2.89e-38, Kruskal–Wallis test, Cohen's d = −1.45). Similar results were observed in the BLA for GFD–GSF (P = 9.02e-09, Wilcoxon test, P = 7.07e-12, Kruskal–Wallis test, Cohen's d = −0.70) and JAD–JAS (P = 2.24e-07, Wilcoxon test, P = 1.37e-12, Kruskal–Wallis test, Cohen's d = −0.62).

In contrast to the amygdala, the hippocampus showed markedly reduced saccade-related activity, except for the increased postsaccadic gamma in both GF and JA conditions. Significant differences

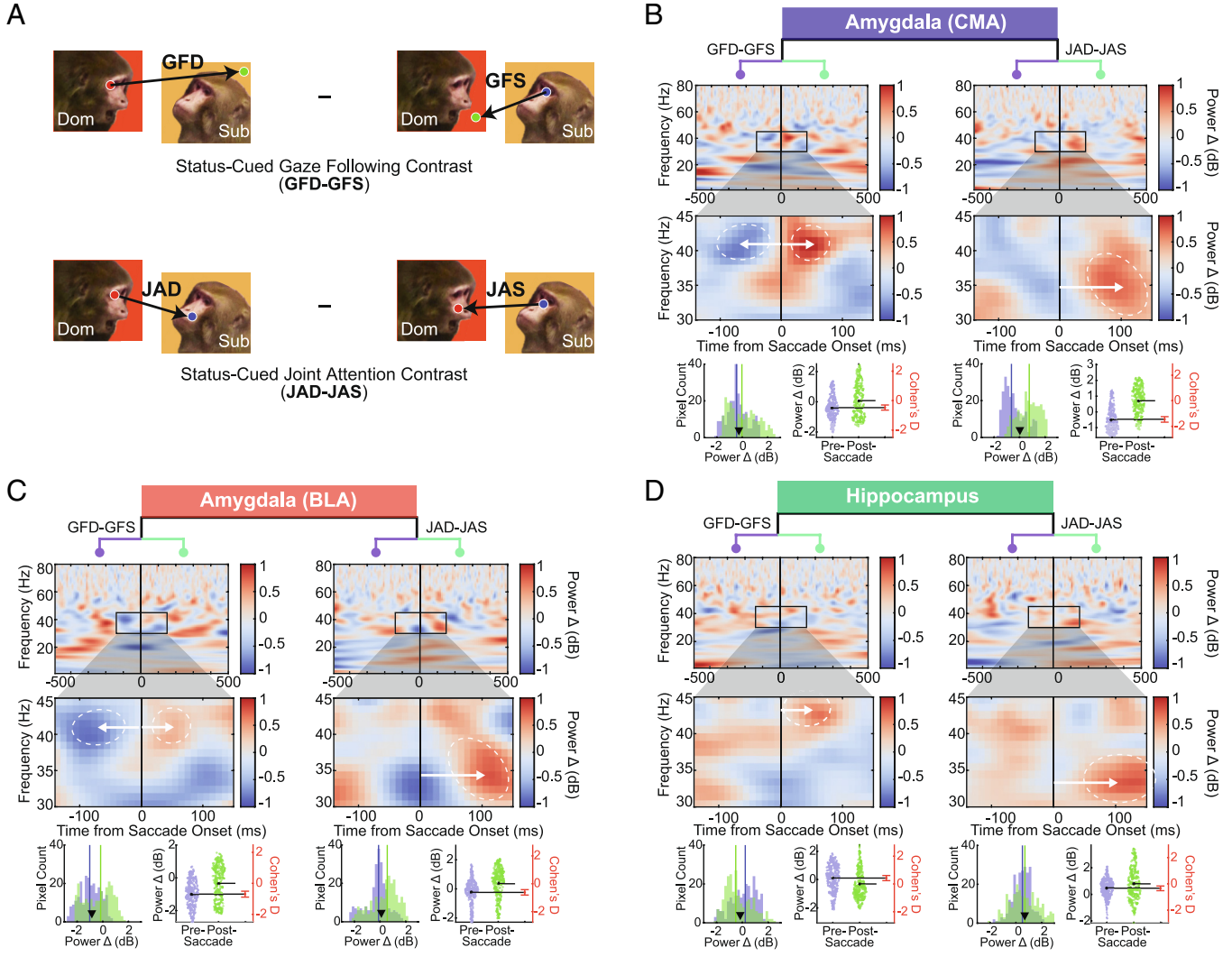

Fig. 4. Gamma and beta power differentiate the social status of individuals who induce GF and JA saccades. (*A*) Schematic of saccade contrasts: GFD–GFS (*Top*) compares GF saccades aligned with the gaze of a dominant vs. a subordinate; JAD–JAS (*Bottom*) compares JA saccades initiated from the face of a dominant vs. a subordinate. (*B*) GF-related power transients in TFHDs computed from LFPs in the CMA. The magnitude of the difference (in dB) is mapped to the color scale shown on the right. To capture the most prominent effects, TFHDs in each panel are zoomed into a smaller time window (−150 ms to 150 ms centered on the saccade onset) and frequency range (15 to 30 Hz). *Inset* plots below each TFHD show the distributions of pixel values in the presaccadic (purple) and postsaccadic (green) periods from two perspectives (*Left*) and the overall distribution across both (*Right*). Under the distributions are Gardner-Altman plots of the data distributions and corresponding Cohen's D effect size estimates. Left columns: Difference between average TFHs of GF saccades from dominant minus subordinate (GFD–GFS). Right columns: Difference between average TFHs of JA saccades with dominant minus subordinate (JAD–JAS). (*C* and *D*) The same as in *B* for the BLA and the hippocampus, respectively.

were found for GFD–GFS (P = 3.54e-05, Wilcoxon test, P = 2.86e-07, Kruskal–Wallis test, Cohen's d = 0.42) and for JAD–JAS (P = 2.53e-3, Wilcoxon test, P = 0.01, Kruskal–Wallis test, Cohen's d = −0.33). The gamma deflection shifted the overall gamma power distribution negatively during GFs in both CMA and BLA (GFD–GFS: median = −0.35, P = 9.35e-05, Wilcoxon test). In contrast, the distribution remained more central during JAs (JAD–JAS: median = 0.06, P = 0.03 in CMA; median = 0.05, P = 0.07 in BLA; Wilcoxon tests).

Discussion

Compared to the deep understanding of the neural machinery that generates saccades as trained, operant behaviors (36), little is known about how saccades are controlled during the spontaneous visual scanning of natural social scenes. During natural vision, saccades sample the elements of the visual scene that serve the behavioral agenda of the organism (37). Here we show that, indeed, the eye movements of viewers of hierarchical social interactions track the exchange of dominant–subordinate signals to extract the perceived relationship between the observed individuals (3, 9).

In our paradigm, status-driven saccades were associated with short transient increases in relative LFP power in the amygdala and hippocampus. These transient oscillatory power increases likely represent changes in network excitability that may amplify or suppress the visual processing of the current or upcoming fixations (38, 39). As shown in Fig. 3, looking from the subordinate to the dominant caused a presaccadic boost in the 20 to 25 Hz (beta) frequency band, as though anticipating the fixation on the dominant. This finding is consistent with the role of the amygdala in orienting visual attention toward the eyes in faces (16, 17) or features in a visual scene that predict positive or negative outcomes (22). By contrast, the power transients associated with gaze shifts from the dominant to the subordinate were primarily postsaccadic, peaking in the initial period of fixation that may represent an active, attentive period of visual processing, possibly due to predictive remapping (40). During fixation on the subordinate, the viewer can detect the effect of the dominant's aggressive displays toward the subordinate. Interestingly, these simple gaze shifts between the dominant and subordinate did not elicit comparable power boost in the anterior hippocampus. It is possible that more caudal regions of the hippocampus would show different saccade-related bursts in these frequency bands.

However, the hippocampus and both nuclear groups in the amygdala showed LFP transients during GF and JA saccades, which are the hallmark of the viewer's social-cognitive engagement with the videos (note that both GF and JA saccades extend in the direction of the observed animal's gaze but only the JA saccades land on the face of the social partner) (Fig. 1 *C* and *F*). Replicating earlier observations (9), the subordinate's fearful, appeasing facial expressions were more likely to engage the viewer in JA than the threatening displays of the dominant. Note that JA with the subordinate, which leads to fixation on the dominant, elicits a brief power transient of anticipatory gamma in the amygdala (Fig. 4 *B–D*). When this gamma boost is subtracted from the gamma boost associated with the opposite saccades (JA with the dominant), the result is a decreased presaccadic gamma (in blue) (Fig. 4 *B–D*). This negative deflection of gamma is followed by a postsaccadic burst of increased gamma that coincides with the initial period of a fixation on the dominant. The GF power transients were 5 to 10 Hz higher in frequency than the JA power transients (Fig. 4 *B–D*). The overall pattern emerging from the analysis of these saccades is the anticipatory, status-dependent component of the high beta (25 to 30 Hz) and low gamma (30 to 45 Hz) transients before saccade onset, followed by a status-independent component of gamma after fixation onset sensitive to having switched the focus to the other monkey as opposed to exploring the same monkey. Again, these findings suggest the presence of a phenomenon akin to predictive remapping (40).

Previous studies in monkeys localized the GF hub of the social brain to the cortex of the superior temporal sulcus, where neurons link information on the other's gaze with distinct targets (41). It is possible that multiple networks of neurons contribute to GF and JA saccades, as is the case with eye contact that activates neurons both in the amygdala and the medial prefrontal cortex (42, 43). The power transients in the amygdala may represent attentional shifts originating from the frontal eye fields that select the targets of the next fixation in the scanpaths (44) or supplementary and presupplementary motor areas (45–47). Indeed, in macaques, strong connections exist between the amygdala and oculomotor and preoculomotor areas of the frontal cortex that are involved in the exploration of faces (48, 49). It has been proposed that a corollary discharge originating from oculomotor areas ensures visual continuity (or perceptual stability), and the anticipatory shifts (remapping) of visual receptive fields from the current fixation to the location of next fixation, (32, 50–52) which may predict features of the subsequent fixation target. In the present study, this prediction refers to the social status of future fixation targets. As the saccade-related power transients likely correspond to periods of altered excitability in the amygdala and the hippocampus, the corollary discharge may also serve as a synchronization or coordination mechanism between the amygdala and the hippocampus during visual exploration (10).

Gamma oscillations (30 to 70 Hz) have been identified in the rodent BLA that contains feedforward circuits involved in processing the affective significance of environmental stimuli and in activating downstream effector circuits, such as the circuits of the CMA (53, 54). Among other functions, gamma oscillations are related to attention and vigilance (55), specifically attention to threatening faces (56, 57). In both cortical networks and the cortex-like cellular structure of the BLA, gamma oscillations depend on reciprocal interactions between pyramidal and fast-spiking cells (58).

In the context of oculomotor and broader sensorimotor control, intrinsic beta and gamma oscillations make complementary contributions. Beta coherence between anterior cingulate cortex and frontal eye fields increases during saccade preparation and is suppressed perisaccadically, consistent with beta's role in stabilizing the current set (59). Brief beta bursts in the motor cortex likewise index premovement synchronization (60). By contrast, gamma activity is typically linked to processing novel information and initiating updated actions.In our data, gamma power increased during and immediately after saccades in a social-status-dependent manner within the amygdala, and in the hippocampus specifically during joint-attention and gaze-following epochs (Figs. 3 and 4). Although we cannot determine from the present experiment whether the transition from presaccadic beta to peri/postsaccadic gamma is causal for saccade initiation or merely corollary to the trigger mechanism, the pattern suggests that the beta–gamma transition recruits the amygdalo-hippocampal-entorhinal circuit during socially driven exploratory behavior (60). In all TFHDs, the anticipatory beta power was followed by an increased postsaccadic gamma activity, which provides the necessary processing bandwidth for channeling the sensory input to the amygdala after the fixation is shifted between the monkeys. A similar pattern is seen in the TFHDs of the amygdala related to JA and GF saccades, but the pre- and postsaccadic beta- and gamma-boosts are more segregated in time (*SI Appendix*, Fig. S9).

The current study has several limitations. The magnitude of the LFP boosts is moderate in power (±1 dB). Because the subtraction method cancels most of the saccade-related frequency components, the surplus gamma and beta boosts are expected to be small in magnitude. Nevertheless, the consensus across monkeys and recording sessions, as well as the consistent temporal and frequency distributions, render the effects statistically robust. Also, the effect size of the contrast between the different types of saccades is consistently robust (Cohen's d consistently > 0.2). Phase coherence between saccades and hippocampal theta oscillations is expected to occur for visually driven saccades (31) and increase during fixations on faces compared to nonfaces (10). Based on these observations, it would be plausible that socially meaningful targets elicit enhanced phase coherence between saccades and oscillations in the amygdala and/or hippocampus. In this study, although we could replicate the phase relationship between saccades and LFP phase in both regions, we failed to demonstrate its stimulus-specificity (*SI Appendix*, Fig. S10). In addition to the theta band, we observed a significant phase locking between the saccade onset and the oscillatory components of LFP in the beta and gamma frequency bands. However, this phase locking effect on the higher frequency bands was inconsistent between the two monkeys. Instead, we found that the social content of the fixated stimuli was reflected in LFP power, which points to the need to further elucidate the contribution of phase- and power-based neural codes to the differential processing of salient information.

Despite these limitations, the discernible changes induced in the LFPs by different types of socially motivated saccades suggest that the primate amygdala contributes detailed information to the elaboration of saccades to valuable targets. Our findings show that in addition to explicit visual features of complex scenes that predict positive or negative outcomes, the amygdala transmits abstract variables to the saccade-generating network of the primate brain, such as the inferred social status of the observed individuals.

Methods

Subjects and Task. Two adult male macaques, M_A (10 y old, 13.6 kg) and M_D (9 y old, 11.8 kg), viewed videos of simulated pairwise interactions between four monkeys organized into virtual hierarchies (Fig. 1*A*). Pairwise interactions were simulated by juxtaposing videos of two monkeys facing each other, one threatening and the other appeasing (Fig. 1*B*). The facial and bodily displays were timed to suggest a receiving–emitting cycle of dominant–subordinate gestures and postures. The highest-ranking monkeys threatened all others, while the lowest-ranking monkeys showed only submissive behaviors. The mid-ranking monkeys were dominant or subordinate depending on the status of their social partner. We created four distinct hierarchy groups (24 videos), each of which was viewed 58 to 74 times. To eliminate possible side-bias, the videos were flipped left–right and presented for an equal amount of time in each orientation. The videos were displayed on a screen (52 × 28.6 cm) at a resolution of 1920 × 1080 FHD, with the monkey positioned 59 cm from the screen, corresponding to approximately 38 pixels per degree. Each video was played for 6 or 15 s at a frame rate of 25 frames per second, resulting in sequences of 125 or 375 frames, respectively. The face and body areas of each monkey were manually segmented and scored frame by frame. Control videos of equal length and resolution depicted moving objects, such as office supplies and toys. In a recording, videos were displayed in blocks of 36 trials (one trial = one video display). The two subjects completed 740 and 928 trials.

To start the display of a video, the subject monkeys had to fixate for 100 ms on a start cue. The experiment was controlled by MonkeyLogic (https://monkeylogic.nimh.nih.gov/). During the videos, the monkeys could look anywhere, including away from the monitor. After each video, the subjects received a small juice reward of the same amount for all videos. The monkeys were not subjected to food or fluid restriction.

Eye Tracking. Eye movements were recorded with a calibrated infrared eye tracker (ETL-200, ISCAN Inc.) with a sampling rate of 125 Hz. Raw data were initially recorded in millivolts (mV), then converted into pixel coordinates using calibration steps. Our method for identifying saccade or fixation onset leverages the energy of the signal (E), as detailed in equation below, where X denotes the input signal, using n = 30 as window size. This method detects energy shifts that distinguish between saccades and fixations. The onset of saccades and fixations coincided with the time point when the second derivative of the energy signal crossed zero.

$$\left[E_t = \frac{\sum_{k=t-n}^{t+n} \left(X[k] - \mu_t\right)^2}{2n+1}\right]_{t=n+1}^{\text{length}(X)-n} \left(\text{when } \mu_t = \frac{\sum_{k=t-n}^{t+n} X[k]}{2n+1}\right).$$

With a 125 Hz sampling rate the signal refresh occurs every 8 ms. The sampling rate of the eye position channel on our data acquisition system (OmniPlex; Plexon Inc.) was 1 kHz, we eliminated timing inaccuracies by upsampling the eye-tracking signals at 1 kHz. This improved the uniformity of the distributions of saccade and fixation durations, reducing artifacts attributed to the lower sample rate across all recording days. This method is described in detail in our previous work (12).

Saccade Classification. All saccades were sorted based on two sets of criteria (Fig. 1 *B* and *C*).

First, saccades were classified based on status of origin and target of each saccade, with D indicating dominant and S indicating subordinate. We discriminated among four types of saccades (Fig. 1*B*): DD, from and to dominant areas; DS, from dominant to subordinate areas; SD, from subordinate to dominant areas; SS, from and to subordinate areas.

Second, we identified four classes of GF and JA saccades based on the status of the monkey that triggered those saccades (Fig. 4). GFD and GFS denote saccades originating from the face area of the dominant or subordinate, respectively, extending within ±30° of that monkey's gaze direction and landing outside face or body regions of the partner. JAD and JAS denote saccades originating from the face area of the dominant or subordinate, respectively, within ±30° of the initiator's gaze direction and landing inside face/body of the partner.

In addition, we classified saccade types of DD, DS, SD, and SS in the control videos depicting pairs of moving objects, where each object was arbitrarily assigned the D or S role. As additional controls, we also marked saccades made by the viewer monkeys on the blank screen between trials (Type 00).

Neural Recordings. We recorded LFPs from two 32-channel linear arrays (V-probes) custom manufactured by Plexon Inc. with contacts distributed on length of 6.5 mm to span the entire dorsoventral expanse of the monkey amygdala. As summarized in *SI Appendix*, Table S2, we recorded LFPs from 187 channels in the CMA (including the central and medial nuclei), 333 channels from the BLA (including the lateral, basal, and accessory basal nuclei), and 214 channels from the subregions of the anterior hippocampus. We used CAR to remove the contamination of the signal from the ocular dipole and the ocular-muscle EMG (24) by subtracting from all the channels the average raw LFP and retain for analysis only the difference between the recorded signal and the common average as shown in Fig. 2. The resulting signal represents the neural activity of a local, mesoscale network of neurons (25, 26).

Processing of the Event Related Potentials. After subtracting the CAR, the data were denoised by setting amplitudes greater than 0.5 μV in absolute value to zero. Subsequently, the denoised LFPs were z-scored (to achieve a baseline amplitude of zero and ensure that each channel contributes equally to the result) and averaged across channels within the CMA, BLA, and HIPP. To obtain smoother waveforms for the ERP analysis, we applied a 0.1 to 50 Hz wide band filter (forward–backward digital Butterworth filter, order = 10), and a Savitzky–Golay filter (order = 2, filter window = 10 ms) to the averaged signals. Next, we carried out an event-triggered analysis on the preprocessed signals, using the following categories of events: 1) saccades produced while watching the monkey hierarchy videos, which were further classified in DD, DS, SD, and SS; 2) saccades produced while watching the object videos, and 3) saccades produced during intervals between trial blocks on the blank screen (type 00).

For each type of saccade, we extracted segments of the preprocessed LFPs in a [−100, 300] ms window, where time 0 corresponded to saccade onset. To assess the selectivity of ERPs for the social content of the fixated visual details, we ran two-sample Welch's t tests pointwise in these time intervals. We compared

ERPs elicited by saccades and fixations on stimuli (monkeys and objects) vs. the black screen (Fig. 2*E*), monkeys vs. objects (Fig. 2*D*), and on the dominant vs. the subordinate monkeys (Fig. 2*C*), with each sample pooled across all subjects and trials. To demonstrate these differences visually, we computed the mean and SEM of ERPs across all subjects, trials, and saccades of the same type.

Extraction of the Power Spectrum. We segmented the preprocessed LFPs according to trial blocks, so that one data segment included a continuous interval from the beginning to the end of a sequence of trials in which the same type of stimulus was presented repeatedly. We divided these segments into three categories according to stimulus type (monkey videos, object videos, and blank screen). Next, we computed the power spectrum of each segment using the fast Fourier-transform. We then summed up the obtained spectral density values in 0.5 Hz bins between 0.5 and 100 Hz and divided by the total sum within this frequency range to obtain relative powers. This yielded two data arrays: the series of frequencies and the corresponding power values.

We then identified the pink noise component by fitting a linear (OLS) regression to the logarithm of frequencies to predict the associated log powers:

$$\log\ y = \beta\ \log\ f + c.$$

To remove the pink noise from the power spectrum and obtain the denoised powers, we subtracted the exponential values predicted by the model from clipping the difference at zero from below, where $\hat{y}$ denotes the predictions, given parameter estimates $\hat{\beta}$ and $\hat{c}$:

$$y' = \max\left\{ y - e^{\hat{y}}, 0 \right\} (\text{when } \hat{y} = \hat{\beta} \log f + \hat{c}).$$

Finally, we computed the mean and SEM of both the raw and denoised power spectra separately for the three types of stimuli and the three regions of interest (CMA, BLA, and HIPP), pooled across subjects and sessions.

Time–Frequency Analysis. To correlate the occurrence of saccades to potential spectral changes in neural activity, we carried out an event-triggered time–frequency analysis. Using wavelet-transform with the Morlet wavelet, we computed time–frequency histograms (TFHs) separately for each channel between 0.1 to 80 Hz (in 1 Hz increments) in 1 s segments (divided into 10 ms windows) of LFPs centered on saccade onset, encompassing the time interval of −500 ms to +500 ms relative to saccade onset. Note that because multiple saccades may happen within a 1 s time window, a given epoch might have contained preceding or subsequent saccades. We then averaged these TFHs across all the electrodes in the CMA, BLA, and hippocampus. Then, the TFHs were averaged across trials by saccade types for every recording session. At the next level of data aggregation, we averaged over all the TFHs across subjects and recording sessions, obtaining one grand average TFH for each saccade type and anatomical region of interest.

Next, we computed the difference between the TFHs aligned to different saccade types to reveal the effect of social hierarchy (i.e., dominant vs. subordinate status of the fixated monkeys). The difference was represented by the Time–Frequency Histogram Difference or TFHD, explained below. The rationale behind this subtraction method was the following: If we want to extract the effect of social hierarchy during shifting the gaze between dominant and subordinate monkeys, we have to subtract the average TFHs triggered by saccades within the same monkey from the average TFHs triggered by saccades to the other monkey of a different social status. Specifically, to unmask the effect of saccades targeting a subordinate monkey, we computed the difference of TFHs between DD and DS saccades. In contrast, to unmask the effect of saccades targeting the dominant, we computed the difference of TFHs between SD and SS saccades. The difference in the presaccade half of the TFHs reflects the effect of anticipation of new visual information, while the difference in the postsaccade part might reflect the processing of its features. Using a similar subtraction paradigm, we could unmask the effect of social hierarchy on the TFHs in the JA and GF conditions. The JA effect was quantified as the difference between JAD and JAS. Likewise, the GF effect was computed as the difference between GFD and GFS saccades.

We graphically represented such power spectral density difference (PSDD) as a heatmap of Time–Frequency Histogram Difference (TFHD), using a color scale from blue (negative) to red (positive) through gray (zero) (*SI Appendix*, Fig. S4*A*). While the above-defined −500 to 500 ms and 0.1 to 80 Hz time–frequency window provided a broad overview of saccade-related spectral effects, we narrowed down our domain of interest for further analysis. Based on the peaks in the alpha/beta (~10 to 25 Hz) and low gamma (~35 to 45 Hz) bands in the session-wide power spectrum (Fig. 3*C*), and the observed spectral perturbations around saccades, we focused the analysis on two frequency ranges: 15 to 30 Hz for the effect of social status, and 30 to 45 Hz for the joint attention and gaze following effects. Furthermore, we narrowed down the time frame to −200 to 200 ms relative to saccade onset, to exclude the potential effects of preceding and subsequent saccades. To assess the significance of power differences, we aggregated the pixel values (1 pixel = 10 ms × 1 Hz) separately for the presaccade (−200 to 0 ms) and postsaccade (0 to 200 ms) intervals, disregarding their topography within these domains.

To quantify the effect of social hierarchy on the power spectrum, we analyzed the TFHs at two levels: background and foreground activity levels. For asserting background modulation (*SI Appendix*, Fig. S4*B*), we tested whether the overall PSDD in the −200 to 200 ms window around saccades was significantly shifted in either direction relative to zero, where zero represented no difference between the compared conditions. Let TFH = TFH_1 – THF_2, where TFH_1 and THF_2 denote the two histograms being subtracted, and TFH the resulting difference. A positive background effect indicates a significant power increase in TFH_1 relative to TFH_2, while a negative background effect indicates a significant power increase in TFH_2 relative to TFH_1. For the foreground effect (*SI Appendix*, Fig. S4*C*), we compared the PSDDs between the presaccadic and the postsaccadic interval under different saccade conditions. If power differences between the two saccade types are asymmetric around saccade onset, the pre- and postsaccadic PSDDs are expected to differ significantly from each other.

Our first H_{01} hypothesis was the lack of background modulation around saccades, i.e., the mean or median of the overall PSDD should not be different from 0. The second H_{02} hypothesis was the lack of difference in PSDD between the presaccadic and postsaccadic time intervals. All combinations of the foreground–background effect were possible. By rejecting the $H_{01,}$ we accept the alternative that there is a perisaccadic modulation of power depending on the viewing condition. By rejecting the H_{02}, we accept the alternative that the power difference is asymmetric between the presaccadic and postsaccadic intervals. The two types of hypothesis tests were carried out by using the nonparametric Wilcoxon rank-sum test. We report the *z*-values, along with the *P*-values and the degrees of freedom (*df*).

Phase Coherence Analysis. To compute the phase coherence of the different oscillations around saccades, we applied bandpass filters to the preprocessed LFPs in the three anatomical regions of interest (CMA, BLA, and HPC) using a 4 Hz bandwidth with the starting frequency ranging from 0 to 50 Hz and 1 Hz stride. Next, we extracted the instantaneous phase of the filtered signals with the help of the Hilbert transform. Saccades were grouped according to stimulus condition (hierarchy videos, object videos, blank screen). The first saccades were removed from each trial to decouple the effect of eye movements during natural viewing from visually evoked responses related to the onset of video presentation. We collected phases at saccade onset and computed the resultant vector, separately for each subject and stimulus condition, using the following formula:

$$v = \frac{1}{N} \sum_{n=1}^{N} e^{i\phi_n},$$

where v is the resultant vector, n iterates over all saccades, N is the total number of saccades, and ϕ_n is the phase at the onset of the nth saccade. We quantified phase coherence as the length, mean resultant length (MRL), and the preferred phase (i.e., the phase at which saccades are the most likely to occur) as the angle of the resultant vector. We identified the peak frequencies of phase coherence through visual inspection and concluded that these frequencies were reasonably similar across anatomical regions and stimulus conditions within the same subject but differed across subjects.

To assess the significance of phase coherence, we constructed 100 surrogate datasets by randomly shuffling the order of saccades within recordings, while keeping the overall distribution of intersaccade intervals constant. We computed MRLs for the surrogate datasets to obtain an empirical

Null-distribution. We considered phase coherence significant in a given time–frequency bin if the associated true MRL exceeded the 95th percentile of the Null-distribution. For visualization purposes, we computed the z-score of the true MRL by subtracting the mean of the surrogate distributions and dividing by their SD. Note that the MRL metric is highly sensitive to sample size, and the number of saccades differed considerably across subjects and stimulus conditions due to the design of trials and behavioral characteristics, which is why MRLs are not directly comparable between these categories. However, the sample size of surrogate datasets always matched the true sample size, rendering the z-scores and p-values computed based on them more suitable for comparison.

Statistical Analysis. Statistical analysis was done using MATLAB and Python. Nonparametric tests were performed across all data.

Data, Materials, and Software Availability. All data and analysis code supporting the findings of this study have been deposited in the public repository Figshare (61) and made available upon publication.

ACKNOWLEDGMENTS. We acknowledge Lizzie Hillier and Derek O'Neill for preparing the monkeys for the experiments. Tess Champ and Dr. Tapas Arakeri helped with recordings and setting up the eye tracker. This work was supported by NIH Grants P50MH100023 and R01MH135267.

Author affiliations: [a]Department of Neurosurgery, Massachusetts General Hospital, Harvard Medical School, Boston, MA 02114; [b]Department of Physiology, College of Medicine, The University of Arizona, Tucson, AZ 85724; [c]Department of Neurology, Dell Medical School, University of Texas at Austin, Austin, TX 78712; [d]Institute of Psychology, ELTE Eötvös Loránd University, Budapest 1075, Hungary; and [e]Zeto, Inc., Santa Clara, CA 95054

1. D. Kumaran, A. Banino, C. Blundell, D. Hassabis, P. Dayan, Computations underlying social hierarchy learning: Distinct neural mechanisms for updating and representing self-relevant information. *Neuron* **92**, 1135–1147 (2016).
2. J. Munuera, M. Rigotti, C. D. Salzman, Shared neural coding for social hierarchy and reward value in primate amygdala. *Nat. Neurosci.* **21**, 415–423 (2018).
3. S. H. Lee, U. Rutishauser, K. M. Gothard, Social status as a latent variable in the amygdala of observers of social interactions. *Neuron* **112**, 3867–3876.e3 (2024).
4. R. W. Wrangham, T. T. Struhsaker, *Primate Societies* (University of Chicago Press, Chicago, IL, 1987).
5. D. L. Cheney, R. M. Seyfarth, The representation of social relations by monkeys. *Cognition* **37**, 167–196 (1990).
6. C. F. Zink *et al.*, Know your place: Neural processing of social hierarchy in humans. *Neuron* **58**, 273–283 (2008).
7. J. F. Dovidio, S. L. Ellyson, Decoding visual dominance: Attributions of power based on relative percentages of looking while speaking and looking while listening. *Soc. Psychol. Q.* **45**, 106 (1982).
8. M. J. Cole, J. Gwizdka, C. Liu, N. J. Belkin, X. Zhang, Inferring user knowledge level from eye movement patterns. *Inf. Process. Manage.* **49**, 1075–1091 (2013).
9. T. M. Champ *et al.*, Social engagement revealed by gaze following in third-party observers of simulated social conflict. *Front. Psychol.* **13**, 952390 (2022).
10. T. Staudigl, J. Minxha, A. N. Mamelak, K. M. Gothard, U. Rutishauser, Saccade-related neural communication in the human medial temporal lobe is modulated by the social relevance of stimuli. *Sci. Adv.* **8**, 6037 (2022).
11. N. J. Emery, The eyes have it: The neuroethology, function and evolution of social gaze. *Neurosci. Biobehav. Rev.* **24**, 581–604 (2000).
12. S. V. Shepherd, Following gaze: Gaze-following behavior as a window into social cognition. *Front. Integr. Neurosci.* **4**, 1254 (2010).
13. D. R. Carney, The nonverbal expression of power, status, and dominance. *Curr. Opin. Psychol.* **33**, 256–264 (2020).
14. U. Rutishauser, A. N. Mamelak, R. Adolphs, The primate amygdala in social perception–Insights from electrophysiological recordings and stimulation. *Trends Neurosci.* **38**, 295–306 (2015).
15. K. M. Gothard, Multidimensional processing in the amygdala. *Nat. Rev. Neurosci.* **21**, 565–575 (2020).
16. R. Adolphs *et al.*, A mechanism for impaired fear recognition after amygdala damage. *Nature* **433**, 68–72 (2005).
17. J. Taubert *et al.*, Amygdala lesions eliminate viewing preferences for faces in rhesus monkeys. *Proc. Natl. Acad. Sci. U.S.A.* **115**, 8043–8048 (2018).
18. A. Martin, L. R. Santos, What cognitive representations support primate theory of mind? *Trends Cogn. Sci.* **20**, 375–382 (2016).
19. A. G. Rosati, A. M. Arre, M. L. Platt, L. R. Santos, Rhesus monkeys show human-like changes in gaze following across the lifespan. *Proc. R. Soc. B.* **283**, 20160522 (2016).
20. C. Frith, U. Frith, Theory of mind. *Curr. Biol.* **15**, R644–R645 (2005).
21. K. Maeda, J. Kunimatsu, O. Hikosaka, Amygdala activity for the modulation of goal-directed behavior in emotional contexts. *PLoS Biol.* **16**, e2005339 (2018).
22. K. Maeda, K. ichi Inoue, J. Kunimatsu, M. Takada, O. Hikosaka, Primate amygdalo-nigral pathway for boosting oculomotor action in motivating situations. *iScience* **23**, 101194 (2020).
23. J. R. Duhamel, C. L. Colby, M. E. Goldberg, The updating of the representation of visual space in parietal cortex by intended eye movements. *Science* **255**, 90–92 (1992).
24. D. Melcher, C. L. Colby, Trans-saccadic perception. *Trends Cogn. Sci.* **12**, 466–473 (2008).
25. P. Cavanagh, A. R. Hunt, A. Afraz, M. Rolfs, Visual stability based on remapping of attention pointers. *Trends Cogn. Sci.* **14**, 147–153 (2010).
26. S. Denagamage, M. P. Morton, N. V. Hudson, A. S. Nandy, Widespread receptive field remapping in early primate visual cortex. *Cell Rep.* **43**, 114557 (2024).
27. S. Neupane, D. Guitton, C. C. Pack, Two distinct types of remapping in primate cortical area V4. *Nat. Commun.* **7**, 1–11 (2016).
28. M. Zirnsak, N. A. Steinmetz, B. Noudoost, K. Z. Xu, T. Moore, Visual space is compressed in prefrontal cortex before eye movements. *Nature* **507**, 504–507 (2014).
29. H. M. Rao, J. P. Mayo, M. A. Sommer, Circuits for presaccadic visual remapping. *J. Neurophysiol.* **116**, 2624–2636 (2016).
30. K. L. Hoffman *et al.*, Saccades during visual exploration align hippocampal 3–8 Hz rhythms in human and non-human primates. *Front. Syst. Neurosci.* **7**, 55656 (2013).
31. M. J. Jutras, P. Fries, E. A. Buffalo, Oscillatory activity in the monkey hippocampus during visual exploration and memory formation. *Proc. Natl. Acad. Sci. U.S.A.* **110**, 13144–13149 (2013).
32. C. N. Katz *et al.*, A corollary discharge mediates saccade-related inhibition of single units in mnemonic structures of the human brain. *Curr. Biol.* **32**, 3082–3094.e4 (2022).
33. C. K. Kovach *et al.*, Manifestation of ocular-muscle EMG contamination in human intracranial recordings. *Neuroimage* **54**, 213–233 (2011).
34. G. Buzsáki, C. A. Anastassiou, C. Koch, The origin of extracellular fields and currents–EEG, ECoG, LFP and spikes. *Nat. Rev. Neurosci.* **13**, 407–420 (2012).
35. B. Pesaran *et al.*, Investigating large-scale brain dynamics using field potential recordings: Analysis and interpretation. *Nat. Neurosci.* **21**, 903–919 (2018).
36. C. J. Bruce, M. E. Goldberg, Physiology of the frontal eye fields. *Trends Neurosci.* **7**, 436–441 (1984).
37. C. T. Miller *et al.*, Natural behavior is the language of the brain. *Curr. Biol.* **32**, R482–R493 (2022).
38. C. E. Schroeder, D. A. Wilson, T. Radman, H. Scharfman, P. Lakatos, Dynamics of active sensing and perceptual selection. *Curr. Opin. Neurobiol.* **20**, 172–176 (2010).
39. C. E. Schroeder, P. Lakatos, Low-frequency neuronal oscillations as instruments of sensory selection. *Trends Neurosci.* **32**, 9–18 (2009).
40. J. D. Golomb, J. A. Mazer, Visual remapping. *Annu. Rev. Vis. Sci.* **7**, 257–277 (2021).
41. H. Ramezanpour, P. Thier, Decoding of the other's focus of attention by a temporal cortex module. *Proc. Natl. Acad. Sci. U.S.A.* **117**, 2663–2670 (2020).
42. C. P. Mosher, P. E. Zimmerman, K. M. Gothard, Neurons in the monkey amygdala detect eye contact during naturalistic social interactions. *Curr. Biol.* **24**, 2459–2464 (2014).
43. O. Dal Monte *et al.*, Widespread implementations of interactive social gaze neurons in the primate prefrontal–amygdala networks. *Neuron* **110**, 2183–2197 (2022).
44. C. J. Bruce, M. E. Goldberg, Primate frontal eye fields. I. Single neurons discharging before saccades. *J. Neurophysiol.* **53**, 603–635 (1985).
45. O. Hikosaka, M. Isoda, Brain mechanisms for switching from automatic to controlled eye movements. *Prog. Brain Res.* **171**, 375–382 (2008).
46. N. Toschi, A. Duggento, L. Passamonti, Functional connectivity in amygdalar–sensory/(pre) motor networks at rest: New evidence from the Human Connectome Project. *Eur. J. Neurosci.* **45**, 1224–1229 (2017).
47. J. D. Schall, Neuronal activity related to visually guided saccadic eye movements in the supplementary motor area of rhesus monkeys. *J. Neurophysiol.* **66**, 530–558 (1991).
48. M. Gerbella, E. Borra, S. Rozzi, G. Luppino, Connections of the macaque granular frontal opercular (GrFO) area: A possible neural substrate for the contribution of limbic inputs for controlling hand and face/mouth actions. *Brain Struct. Funct.* **221**, 59–78 (2016).
49. E. Borra, G. Luppino, Large-scale temporo–parieto–frontal networks for motor and cognitive motor functions in the primate brain. *Cortex* **118**, 19–37 (2019).
50. M. A. Sommer, R. H. Wurtz, Brain circuits for the internal monitoring of movements. *Annu. Rev. Neurosci.* **31**, 317–338 (2008).
51. R. H. Wurtz, Corollary discharge contributions to perceptual continuity across saccades. *Annu. Rev. Vis. Sci.* **4**, 215–237 (2018).
52. J. Martinez-Trujillo, Corollary discharge: Linking saccades and memory circuits in the human brain. *Curr. Biol.* **32**, R774–R776 (2022).
53. A. Amir, D. B. Headley, S. C. Lee, D. Haufler, D. Pare, Vigilance-associated gamma oscillations coordinate the ensemble activity of basolateral amygdala neurons. *Neuron* **97**, 656–669 (2018).
54. D. B. Headley, P. Kyriazi, F. Feng, S. S. Nair, D. Pare, Gamma oscillations in the basolateral amygdala: Localization, microcircuitry, and behavioral correlates. *J. Neurosci.* **41**, 6087–6101 (2021).
55. A. K. Engel, W. Singer, Temporal binding and the neural correlates of sensory awareness. *Trends Cogn. Sci.* **5**, 16–25 (2001).
56. Q. Luo, T. Holroyd, M. Jones, T. Hendler, J. Blair, Neural dynamics for facial threat processing as revealed by gamma band synchronization using MEG. *Neuroimage* **34**, 839–847 (2007).
57. H. Oya, H. Kawasaki, M. A. Howard, R. Adolphs, Electrophysiological responses in the human amygdala discriminate emotion categories of complex visual stimuli. *J. Neurosci.* **22**, 9502–9512 (2002).
58. G. Buzsáki, X. J. Wang, Mechanisms of gamma oscillations. *Annu. Rev. Neurosci.* **35**, 203–225 (2012).
59. S. Babapoor-Farrokhran, M. Vinck, T. Womelsdorf, S. Everling, Theta and beta synchrony coordinate frontal eye fields and anterior cingulate cortex during sensorimotor mapping. *Nat. Commun.* **8**, 13967 (2017).
60. S. Little, J. Bonaiuto, G. Barnes, S. Bestmann, Human motor cortical beta bursts relate to movement planning and response errors. *PLoS Biol.* **17**, e3000479 (2019).
61. S. Lee, "Lee *et al.*, Saccade-related LFP power transients in the primate amygdala and hippocampus linked to the perception of social status, data and analysis code." Figshare. https://doi.org/10.6084/m9.figshare.29206241. Deposited 16 December 2025.